Research Square

Preprints are preliminary reports that have not undergone peer review.
They should not be considered conclusive, used to inform clinical practice,
or referenced by the media as validated information.

Continuum coupling and the exact reflection phase of two-dimensional surface polaritons at a conducting sheet edge

Ji-Hun Kang

jihunkang@kongju.ac.kr

Kongju National University

Research Article

Keywords: surface polariton, edge reflection, coupled-mode theory, evanescent continuum

Posted Date: November 23rd, 2026

DOI: https://doi.org/10.21203/rs.3.rs-11643673/v1

License: This work is licensed under a Creative Commons Attribution 4.0 International License.
Read Full License

Additional Declarations: No competing interests reported.

Continuum coupling and the exact reflection phase of two-dimensional surface polaritons at a conducting sheet edge

Ji-Hun Kang[1,2,3,4*]

[1] Department of Optical Engineering, Kongju National University, Cheonan 31080, Republic of Korea

[2] Department of Future Convergence Engineering, Kongju National University, Cheonan 31080, Republic of Korea

[3] Institute of Application and Fusion for Light, Kongju National University, Cheonan 31080, Republic of Korea

[4] School of Applied and Engineering Physics, Cornell University, Ithaca, New York 14853, USA

Corresponding author: *jihunkang@kongju.ac.kr

In this paper, we provide a theoretical description of how the reflection phase of a two-dimensional surface polariton (2DSP) is governed by the evanescent continuum excited at the edge of a 2D conducting sheet. Exact scattering amplitudes for a sheet termination have been obtained through the Wiener-Hopf (WH) method, while approximate modal descriptions have been studied using coupled-mode theory (CMT). Here, we solve the complete CMT integral equations to connect the reflection phase directly to the modal coupling between the surface-bound 2D polariton and the unbound continua on the two sides of the termination. In the local lossless quasistatic limit, eliminating the continuum amplitudes yields a positive effective reactive response whose separate terms characterize the two evanescent continua. We show that this positive structure determines the direction of the phase modification produced when the sheet-side continuum is restored, reducing the reactive response and shifting the potential reflection phase to $\pi/4$. Furthermore, by solving the coupled modal integral equations analytically, we obtain the exact normalized continuum amplitudes and demonstrate that their superposition brings the surface current continuously to zero at the edge while producing an inverse-square-root singularity in the normal electric field. By solving the modal equations at successive sheet-side continuum cutoffs while retaining the complete empty-side continuum, we also examine how these localized near-edge fields govern the convergence of the reflected phase. Our findings unite the exactness of the WH

solution with the physical transparency of CMT and provide quantitative phase-convergence criteria for this one-sided continuum truncation scheme.

Keywords: surface polariton; edge reflection; coupled-mode theory; evanescent continuum;

Introduction

When a surface polariton propagating along a two-dimensional (2D) conducting sheet [1,2] encounters a sharp termination, its reflection at the edge determines both the standing-wave profile and the resonance condition of a finite resonator [3,4]. Consequently, the reflection phase carries essential information about how the electromagnetic field adjusts to the structural discontinuity. In the proximity of the edge, this field adjustment involves the excitation of unbound evanescent fields spanning a broad range of spatial scales [5]. Understanding how these localized evanescent fields couple to the propagating surface polariton is therefore crucial for connecting the near-edge field rearrangement to the reflection phase observed in the far field.

The anomalous reflection phase of graphene plasmons and the essential role of the near-edge evanescent field were discussed in previous studies [6], and subsequent theoretical studies based on the Wiener-Hopf (WH) method provided exact quasistatic scattering amplitudes for 2D conductivity junctions, including the bare conducting edge as a limiting case [7,8]. In addition, the edge reflection of 2D surface polaritons (2DSPs) was interpreted in terms of an effective impedance and the interference between polaritonic and evanescent fields [9].

Each of these two approaches has distinct advantages and limitations. While the WH method yields exact analytical expressions for the reflection coefficient, it operates on global Fourier-transformed fields in the complex momentum plane, which obscures the individual roles of the surface-bound polariton and the distinct unbound continuum modes on the two sides of the edge. Conversely, a representation based on CMT is particularly advantageous for physical interpretation, because its basic building blocks are complete sets of orthonormal transverse eigenvectors defined in each region of space [10–12]. In practice, however, solving the coupled singular integral equations of CMT is challenging, so previous CMT studies have relied on single-mode approximations [6], diagonal continuum approximations that neglect off-diagonal continuum coupling [12], or numerical discretization with finite momentum cutoffs [10]. Consequently, it has remained unclear how the complete CMT reproduces the exact reflection phase and resolves the near-edge field singularities, and how much of the high-momentum continuum must be retained in numerical CMT calculations to achieve phase convergence.

In this paper, we bridge this gap by deriving the exact analytical solution of the bare-edge reflection problem directly within the complete CMT, thereby combining the analytical exactness of the WH result with the modal transparency of CMT. Using this exact modal solution, we connect three key physical quantities within a unified calculation: the continuum contribution to the boundary response, the reflection phase shift, and the spatial profile of the surface current near the termination. By combining the continuum responses at the interface, we separate the contributions arising from the sheet-side and empty-side continua and show that the positive decay responses of the continuum modes fix the sign of the phase correction when sheet-side continuum modes are restored. Using the exact continuum amplitudes, we then demonstrate how the same modal readjustment brings the surface current continuously to zero at the edge. Moreover, by solving the projected CMT equations across a sequence of sheet-side momentum cutoffs while retaining the complete empty-side continuum, we quantitatively establish the spectral range required to accurately reproduce the exact reflection phase.

Theoretical model

1. Coupled-mode formulation at the edge

To establish a self-contained notation, we begin by briefly revisiting the coupled-mode formulation for 2DSP scattering at a structural discontinuity [11,12], adapted here to a bare sheet termination in the quasistatic limit. Consider a 2D conducting sheet located at $z = 0$ and occupying the half-plane $x < 0$, as illustrated in Fig. 1(a). The structure is uniform along the y-direction and is embedded in a homogeneous medium with absolute permittivity ϵ_b and permeability μ_b. We assume that a transverse-magnetic (TM) surface polariton propagates along the $+x$-direction toward the termination at $x = 0$. Under the time-harmonic condition $e^{-i\omega t}$, we consider a local lossless surface conductivity $\sigma = i\sigma_I$ with $\sigma_I > 0$. Then, the characteristic confinement scale κ and the dimensionless parameter ν measuring retardation can be defined as

$$\kappa = \frac{2i\omega\epsilon_b}{\sigma} > 0, \quad k_b = \omega\sqrt{\epsilon_b\mu_b}, \quad \nu = \frac{k_b}{\kappa}. \tag{1}$$

Our main analytical results focus on the quasistatic limit ($\nu \to 0$), in which the polariton propagation momentum approaches κ. For completeness, the corresponding retarded modal equations for finite ν are provided in Appendix A. Incorporating material loss, nonlocal conductivity dispersion [13], or microscopic edge reconstructions requires corresponding modifications to the conductivity model and boundary conditions, for which the present solution provides a rigorous analytical baseline.

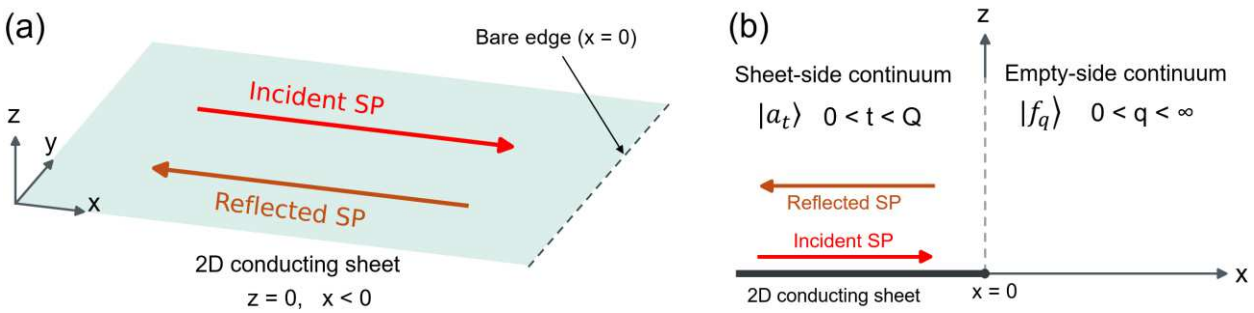


Figure 1: Bare-edge reflection geometry. (a) A normally incident TM surface polariton reaches the edge of a 2D conducting sheet. (b) Cross section and continuum bases used for boundary matching; the sheet-side cutoff is Q, while the empty-side continuum is retained in full.

For TM-polarized waves, the magnetic field has only a y-component H_y that is an odd (anti-symmetric) function of z with respect to the sheet plane at $z = 0$. Therefore, it is sufficient to formulate the problem in the upper half-space $z > 0$ and recover the field in $z < 0$ by odd continuation. From Maxwell's equations, the tangential and normal electric field components are obtained as $E_x = -i\partial_z H_y/(\omega\epsilon_b)$ and $E_z = i\partial_x H_y/(\omega\epsilon_b)$, respectively. Since the discontinuity of the tangential magnetic field across the sheet defines the surface current density $J_x = -2H_y(x, 0^+)$, combining this relation with the constitutive equation $J_x = \sigma E_x$ yields the boundary conditions on the upper surface $z = 0^+$,

$$\partial_z H_y = -\kappa H_y \quad (x < 0, z = 0^+), \quad H_y = 0 \quad (x > 0, z = 0). \tag{2}$$

In the sheet region ($x < 0$), the boundary condition relates the surface value of H_y to its vertical gradient, whereas in the empty region ($x > 0$), anti-symmetry and field continuity across $z = 0$ require the magnetic trace to vanish. As established in Ref. [12], these two distinct boundary conditions define two different complete sets of orthonormal transverse eigenvectors in the two

regions. Across the vertical interface at $x = 0$, the continuity of the tangential electromagnetic fields requires both H_y and $\partial_x H_y$ to be continuous for all $z > 0$.

To simplify the notation, we introduce the dimensionless coordinates $X = \kappa x$ and $Z = \kappa z$ and adopt the Dirac notation. Let $|p\rangle$ denote the orthonormal eigenvector for the surface-bound polariton, $|a_t\rangle$ denote the unbound anti-symmetric continuum modes on the sheet side, and $|f_q\rangle$ denote the unbound continuum modes on the empty side, where $t > 0$ and $q > 0$ represent dimensionless transverse momenta. Normalized on the half-line $Z > 0$ with the inner product $\langle u|v\rangle = \int_0^\infty \langle u|Z\rangle\langle Z|v\rangle\, dZ$, their real-space representations are given by

$$\langle Z|p\rangle = \sqrt{2}\, e^{-Z}, \qquad \langle Z|a_t\rangle = \sqrt{\frac{2}{\pi}}\, \frac{t\cos(tZ) - \sin(tZ)}{\sqrt{1+t^2}}, \quad t > 0, \tag{3}$$

$$\langle Z|f_q\rangle = \sqrt{\frac{2}{\pi}}\, \sin(qZ), \quad q > 0.$$

Here, the eigenvector $|p\rangle$ characterizes the exponentially confined 2DSP, while the continuum eigenvectors $|a_t\rangle$ satisfy the same sheet boundary condition in Eq. (2) and complete the orthonormal transverse basis for $x < 0$. Similarly, the eigenvectors $|f_q\rangle$ form a complete orthonormal basis for the empty region $x > 0$. Because the system is symmetric with respect to $z = 0$, the scattering of the anti-symmetric polariton $|p\rangle$ closes entirely within the anti-symmetric sector. Detailed orthogonality and completeness relations for these bases are summarized in Appendix A.

Following the modal expansion procedure [12], we express the magnetic field in the sheet and empty regions as transverse state vectors $|H_L(X)\rangle$ and $|H_R(X)\rangle$, respectively, such that $H_L(X,Z) = \langle Z|H_L(X)\rangle$ and $H_R(X,Z) = \langle Z|H_R(X)\rangle$. In the quasistatic limit, every continuum component decays exponentially away from the interface at $X = 0$. For an incident polariton with unit amplitude, the field states in the two regions can be expanded as

$$|H_L(X)\rangle = [e^{iX} - Re^{-iX}]|p\rangle - \int_0^\infty \alpha_t |a_t\rangle e^{tX}\, dt,$$
$$|H_R(X)\rangle = \int_0^\infty \phi_q |f_q\rangle e^{-qX}\, dq, \tag{4}$$

where R is the reflection coefficient of the 2DSP, and α_t and ϕ_q are the undetermined modal amplitudes of the sheet-side and empty-side continua, respectively. Because a sheet-side continuum mode of transverse momentum t decays over a characteristic distance $1/(\kappa t)$ from the interface, the high-momentum components ($t \gg 1$) govern the strongly localized near-field profile in the immediate vicinity of the edge.

The coupling between the two regions is governed by the inner products $W_{u\leftarrow v} = \langle u|v\rangle$ between the transverse eigenvectors across the interface. Specifically, the two coupling overlaps required for the present geometry can be explicitly evaluated as

$$P(q) \equiv W_{f_q\leftarrow p} = \langle f_q|p\rangle = \frac{2q}{\sqrt{\pi}(1+q^2)},$$
$$W(q,t) \equiv W_{f_q\leftarrow a_t} = \langle f_q|a_t\rangle = \frac{2qt}{\pi\sqrt{1+t^2}}\,\mathrm{PV}\frac{1}{q^2-t^2} - \frac{\delta(q-t)}{\sqrt{1+t^2}}, \tag{5}$$

with the reverse overlaps satisfying $W_{v\leftarrow u} = W^*_{u\leftarrow v}$. Physically, the coupling factor $P(q)$ projects the incident and reflected polariton profile onto the empty-side continuum modes, whereas the kernel $W(q,t)$ mediates the coupling between the empty-side and sheet-side continua. In particular, the principal-value (PV) term in $W(q,t)$ couples modes with different transverse momenta ($q \neq t$), while the Dirac delta term connects modes of equal transverse momentum ($q = t$). In previous CMT analyses [12], off-diagonal continuum coupling was neglected under a diagonal continuum approximation to obtain a closed-form algebraic estimate, whereas here we retain both contributions to construct the exact solution.

Applying the boundary conditions at $X = 0$, i.e., the continuity of the magnetic field state and its X-derivative (corresponding to the continuity of E_z), yields two coupled equations linking the two vector spaces,

$$(1-R)|p\rangle - \int_0^\infty \alpha_t |a_t\rangle\, dt = \int_0^\infty \phi_q |f_q\rangle\, dq,$$
$$(1+R)|p\rangle + i\int_0^\infty t\alpha_t |a_t\rangle\, dt = i\int_0^\infty q\phi_q |f_q\rangle\, dq. \tag{6}$$

Projecting the first line of Eq. (6) onto $\langle p|$ and $\langle a_t|$, and projecting the second line onto $\langle f_q|$, we obtain the standard coupled modal integral equations,

$$1-R = \int_0^\infty P(q)^*\phi_q\, dq, \quad \alpha_t = -\int_0^\infty W(q,t)^*\phi_q\, dq,$$
$$(1+R)P(q) + i\int_0^\infty tW(q,t)\alpha_t\, dt = iq\phi_q. \tag{7}$$

Equations (1)-(7) complete the review of the CMT formulation and clearly illustrate the underlying modal coupling mechanism. The first two relations in Eq. (7) show that the empty-side continuum amplitude ϕ_q projects back onto the bound mode $|p\rangle$ to determine $1-R$ and onto the sheet-side modes $|a_t\rangle$ to determine α_t, while the derivative condition in the second line couples both continua to $(1+R)$, weighted by their respective spatial decay rates q and t. We now examine the exact boundary response and analytical solution of Eq. (7).

2. How the continuum determines the reflection phase

To understand physically how the two continua determine the reflection coefficient R, let $|h\rangle = |H_R(0)\rangle = |H_L(0)\rangle$ denote the common transverse magnetic-field profile at the matching plane $X=0$. From the field continuity relations in Eq. (7), the expansion coefficients of $|h\rangle$ in the two bases are simply $\langle f_q|h\rangle = \phi_q$, $\langle a_t|h\rangle = -\alpha_t$, and $\langle p|h\rangle = 1-R$. Substituting these relations into the derivative matching condition in Eq. (6) allows us to collect the longitudinal derivative responses of all unbound continuum modes into a single transverse boundary-response operator $\widehat{M}$,

$$\widehat{M} = \int_0^\infty q|f_q\rangle\langle f_q|\, dq + \int_0^\infty t|a_t\rangle\langle a_t|\, dt. \tag{8}$$

Physically, the first term in $\widehat{M}$ represents the spatial decay response of the empty-side evanescent continuum, while the second term represents the corresponding response of the sheet-side evanescent continuum. Because the spatial decay rates q and t are strictly positive for all evanescent modes, every mode on both sides of the edge contributes positively to $\widehat{M}$. The expectation value of $\widehat{M}$ for any boundary state is therefore a sum of squared modal projections weighted by these positive decay rates.

With $\widehat{M}$ defined in Eq. (8), the derivative matching condition in Eq. (6) takes the compact form $(i\widehat{M} + |p\rangle\langle p|)|h\rangle = 2|p\rangle$. Projecting this relation onto $\langle p|\widehat{M}^{-1}$ and using $\langle p|h\rangle = 1 - R$ immediately reduces the coupled continuum problem to an impedance-like scalar relation for the reflection coefficient,

$$R = \frac{1 + i\mathcal{B}}{1 - i\mathcal{B}}, \quad \mathcal{B} = \langle p|\widehat{M}^{-1}|p\rangle, \quad \Phi = \arg(R) = 2\arctan(\mathcal{B}). \tag{9}$$

Here, the real dimensionless parameter $\mathcal{B}$ represents the effective reactive boundary response (analogous to a normalized boundary susceptance) experienced by the surface polariton at the termination. The completeness of the empty-side basis ensures that $\widehat{M}$ is positive-definite so that $\mathcal{B} > 0$. The factor of i in Eq. (9) originates from the longitudinal derivative matching condition, because differentiation multiplies propagating modes by imaginary propagation constants and evanescent modes by real decay rates. This purely reactive coupling guarantees total reflection ($|R| = 1$) in the lossless quasistatic limit, while encoding the effect of the near-edge modal adjustment on far-field scattering in the reflection phase Φ.

The additive structure of $\widehat{M}$ in Eq. (8) provides a clear physical explanation for how each continuum modifies the reflection phase. As a single-mode sheet approximation, if we retain the complete empty-side continuum while neglecting the sheet-side continuum ($|a_t\rangle$), the boundary operator reduces to $\widehat{D} = \int_0^\infty q|f_q\rangle\langle f_q|\, dq$. Since the states $|f_q\rangle$ are mutually orthogonal, $\widehat{D}^{-1}$ acts simply as $1/q$ on each mode, and the baseline response $\mathcal{B}_0$ can be evaluated directly using $P(q)$ from Eq. (5),

$$\mathcal{B}_0 = \langle p|\widehat{D}^{-1}|p\rangle = \int_0^\infty \frac{|P(q)|^2}{q}\, dq = \frac{2}{\pi}, \quad \arg(R_0) = 2\arctan\frac{2}{\pi} \simeq 0.361\pi. \tag{10}$$

This result reproduces the approximation originally introduced in Ref. [6], providing a reference value against which the role of the sheet-side continuum can be measured.

When the sheet-side continuum modes $|a_t\rangle$ are restored, they open additional evanescent channels on the conducting sheet and add the second positive term in Eq. (8). Because adding positive decay channels increases the overall boundary operator $\widehat{M}$ relative to $\widehat{D}$, its inverse response $\mathcal{B} = \langle p|\widehat{M}^{-1}|p\rangle$ to the fixed polariton source $|p\rangle$ must decrease ($\mathcal{B} < \mathcal{B}_0$) [14]. Indeed, evaluating $\mathcal{B}$ with the exact continuum spectra derived in Section 3 gives

$$\mathcal{B} = \sqrt{2} - 1, \qquad \Phi = 2\arctan(\mathcal{B}) = \frac{\pi}{4}. \tag{11}$$

Thus, restoring the sheet-side continuum lowers the reflection phase shift from approximately 65° (0.361π) to 45° (0.25π), a substantial modification of about 20°. A key advantage of our CMT formulation is that it identifies both the specific modal term responsible for this shift and the negative sign of the phase correction purely from physical positivity, even before the exact analytical solution is invoked.

Now, to examine how this phase correction builds up across different spatial scales near the edge, we can retain the sheet-side continuum modes up to a finite momentum cutoff $Q = k_{z,\max}/\kappa$ ($0 < t < Q$) while keeping the full empty-side continuum ($0 < q < \infty$),

$$\widehat{M}_Q = \widehat{D} + \int_0^Q t|a_t\rangle\langle a_t|\, dt, \quad \mathcal{B}_Q = \langle p|\widehat{M}_Q^{-1}|p\rangle. \tag{12}$$

At each cutoff Q, the boundary matching conditions are projected onto the retained modes and solved self-consistently so that all modal amplitudes readjust to the available basis. We note that the resulting cutoff errors characterize this one-sided sheet-continuum truncation and do not directly bound the error when both continua are truncated simultaneously. Because increasing Q progressively adds positive sheet-side modes to $\widehat{M}_Q$, both the reactive response $\mathcal{B}_Q$ and the reflection phase $\Phi_Q = 2\arctan(\mathcal{B}_Q)$ decrease monotonically from their single-mode value at $Q = 0$ toward the exact limit $\Phi = \pi/4$ as $Q \to \infty$.

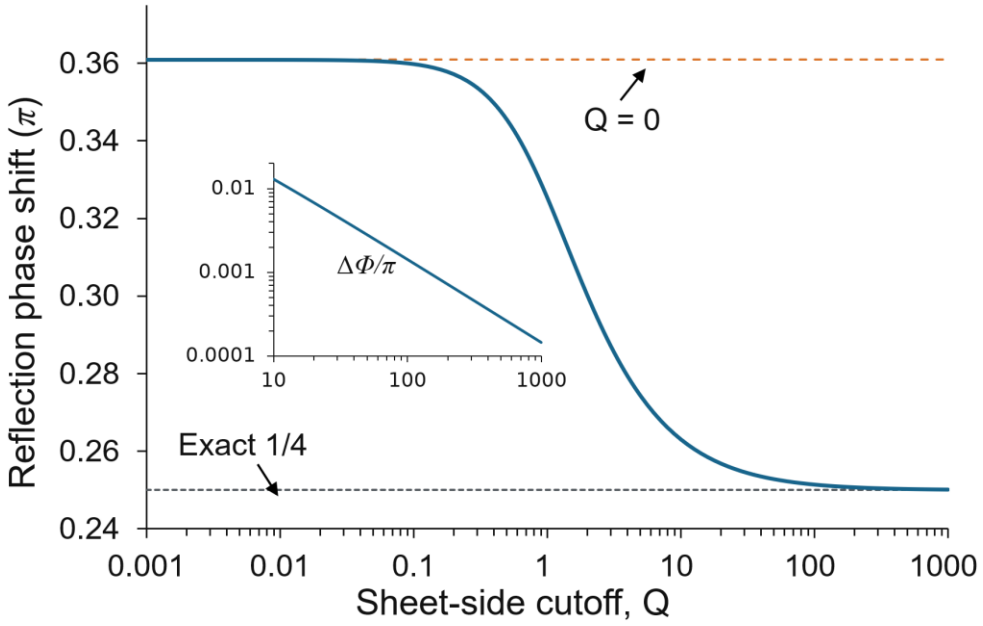


Figure 2: Reflection phase versus the sheet-side continuum cutoff Q, with the complete empty-side continuum retained. The dashed and dotted lines mark $Q = 0$ and the exact phase $\pi/4$, respectively. Inset: phase error, $\Delta\Phi/\pi$, versus Q. The phase convention follows Eq. (4).

Figure 2 demonstrates this monotonic convergence over six decades of the cutoff momentum Q. Specifically, at Q =1, 10, 100, and 1000, the calculated reflection phase Φ_Q reaches about 0.3254π, 0.2631π, 0.2514π, and 0.2501π, respectively, with the residual phase error $\Delta\Phi = \Phi_Q - \pi/4$ numerically approaching a Q^{-1} dependence at large Q (inset of Fig. 2). Under the present one-sided cutoff scheme, choosing $Q \geq 15$ reduces the phase error below 0.01π. It is worth noting that every finite-cutoff approximation ($Q < \infty$) yields a real value of $\mathcal{B}_Q$ and therefore strictly conserves reflected power ($|R_Q| = 1$). Consequently, power conservation alone cannot test whether a modal basis is sufficiently complete in a lossless quasistatic calculation, whereas the reflection phase serves as a sensitive probe of modal completeness. Physically, although high-momentum sheet modes ($t \gg 1$) are localized within a subwavelength distance $\sim (\kappa t)^{-1}$ of the termination, their participation in the boundary matching significantly alters the phase of the reflected polariton in the far field.

3. Exact spectra and the spatial field

We now determine the exact continuum amplitudes by solving the coupled modal equations analytically. In the quasistatic limit, the magnetic field H_y satisfies Laplace's equation in the upper half-space subject to the boundary conditions in Eq. (2). Because the system is lossless and total reflection occurs at the edge, the total field on the sheet side ($s = -X > 0$) forms a standing wave. Formulating the problem in terms of a real standing-wave field $h_L(s, Z)$ allows us to cleanly separate the reflection phase of the bound polariton from the real amplitude distribution of the continuum,

$$h_L(s, Z) = e^{-Z}\sin(s + \theta) - \int_0^\infty \rho(t) e^{-ts}[\cos(tZ) - \frac{\sin(tZ)}{t}]dt. \tag{13}$$

Here, θ is the standing-wave phase parameter of the bound polariton and $\rho(t)$ is the real spectral density of the sheet-side continuum. Note that the bracketed transverse profile in Eq. (13) is directly proportional to the normalized sheet-side eigenvector $\langle Z|a_t\rangle$ in Eq. (3). Specifically, multiplying the real standing-wave solution $h_L(s, Z)$ by the complex normalization factor $-2i\sqrt{2}\, e^{i\theta}$ converts the first term of Eq. (13) into $[e^{iX} - e^{2i\theta}e^{-iX}]\langle Z|p\rangle$, which matches the complex scattering expansion $H_L(X, Z) = \langle Z|H_L(X)\rangle$ in Eq. (4) with unit incident amplitude and reflection coefficient $R = e^{2i\theta}$.

As shown in Appendix B, projecting the continuity of the standing-wave field and its longitudinal derivative at $s = 0$ eliminates the empty-side continuum and reduces the problem to a Cauchy singular integral equation for $\rho(t)$. Requiring the electromagnetic field to remain physically regular at the edge (bounded magnetic field trace and finite local electric-field energy [15]) uniquely fixes the standing-wave phase to $\theta = \pi/8$ and yields closed-form expressions for the continuum densities. Multiplying the standing-wave solution by $-2i\sqrt{2}\, e^{i\pi/8}$ then provides the exact reflection coefficient and normalized modal amplitudes in Eq. (4),

$$R = e^{i\pi/4}, \quad \alpha_t = -i\sqrt{\frac{2}{\pi}}\, e^{i\pi/8}\, \frac{e^{-\eta(t)}}{\sqrt{1+t^2}}, \quad \phi_q = -i\sqrt{\frac{2}{\pi}}\, e^{i\pi/8}\, \frac{e^{\eta(q)}}{1+q^2},$$
$$\eta(t) = \frac{1}{\pi}\int_0^\infty \frac{\log(t+u)}{1+u^2}\, du\,, \quad t > 0. \tag{14}$$

All scattering quantities in Eq. (14) are thus expressed in terms of a single elementary integral $\eta(t)$. Because α_t and ϕ_q are normalized in the orthonormal basis of Eq. (3), they can be substituted directly into the CMT equations of Sections 1 and 2, and used to reconstruct the spatial fields on both sides of the edge. In particular, $R = e^{i\pi/4}$ gives $\mathcal{B} = \tan(\pi/8) = \sqrt{2} - 1$ via Eq. (9), confirming the exact phase shift in Eq. (11). We also note that in the bare-edge limit, the WH solution in Eqs. (1) and (2) of Ref. [8] yields the potential reflection coefficient $r_\varphi = e^{i\pi/4} = R$, in exact agreement with Eq. (14), while the corresponding surface-current and magnetic-field reflection coefficients are $-R = e^{-3i\pi/4}$ as summarized in Appendix A.

Figure 3 shows the magnitudes of the exact continuum amplitudes $|\alpha_t|$ and $|\phi_q|$ across eight decades of the normalized transverse momentum. Because $\eta(t) \sim \frac{1}{2}\log t$ at large momentum ($t \gg 1$), both spectra converge to the same algebraic tail $|\alpha_t|, |\phi_q| \sim \sqrt{2/\pi}\, t^{-3/2}$. These curves reveal how the near-edge evanescent field is distributed across transverse length scales. In particular, the slowly decaying $t^{-3/2}$ high-momentum tails supply the short spatial scales needed to satisfy the boundary conditions right at the termination.

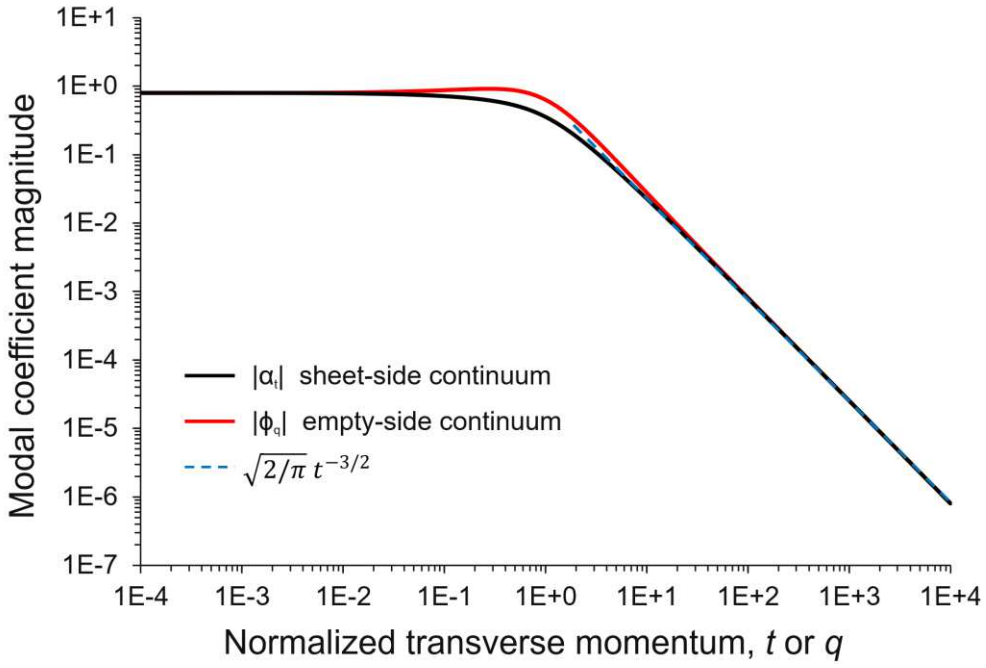


Figure 3: Exact continuum modal amplitudes in the spatial normalization of Eq. (3). The incident surface-bound polariton has unit modal coefficient, corresponding to a surface trace

$\langle Z=0|p\rangle=\sqrt{2}$. Both continuum spectra $|\alpha_t|$ and $|\phi_q|$ approach the common high-momentum power-law tail $\sqrt{2/\pi}\,t^{-3/2}$ (dashed line). These amplitudes weight the orthonormal transverse profiles and govern their spatial decay away from the edge.

The physical necessity of the sheet-side continuum becomes clearer when we examine the magnetic field on the conducting sheet surface ($Z=0^+$), which is directly proportional to the surface current density via $J_x=-2H_y(x,0^+)$. Setting $Z=0$ in Eq. (13) gives the standing-wave surface profile $\psi(s)$, and evaluating the integral of the exact density $\rho(t)$ at the edge ($s=0$) yields an exact sum rule,

$$\psi(s)=h_L(s,0)=\sin(s+\pi/8)-\int_0^\infty \rho(t)e^{-ts}\,dt,\quad \int_0^\infty \rho(t)\,dt=\sin\frac{\pi}{8}, \tag{15}$$

so that $\psi(0)=0$. Physically, if one considers only the surface-bound polariton (the first term in Eq. (15)), the surface magnetic field and surface current fail to vanish at the termination, approaching finite nonzero value at $s=0$. The second relation in Eq. (15) demonstrates that the excited sheet-side continuum modes superimpose at the edge with the exact amplitude required to cancel the bound-wave surface trace, bringing the total surface current continuously to zero ($J_x(0)=0$). Thus, continuous current termination at the edge and the far-field reflection phase shift from 0.361π to $\pi/4$ are two phenomena of the same continuum coupling process. Moreover, the rate at which the surface current vanishes approaching the edge ($s\to 0^+$) is governed directly by the high-momentum tail $\rho(t)\sim t^{-3/2}/(\sqrt{2}\pi)$. Evaluating the Laplace integral in Eq. (15) for $s\to 0^+$ yields the leading near-edge behavior,

$$\psi(s)\sim\sqrt{\frac{2}{\pi}}\,\sqrt{s},\quad \psi'(s)\sim\frac{1}{\sqrt{2\pi s}},\quad s\to 0^+. \tag{16}$$

Multiplying Eq. (16) by the complex normalization factor $-2i\sqrt{2}\,e^{i\pi/8}$ (magnitude $2\sqrt{2}$) gives the corresponding edge scaling for the complex magnetic field at unit incident polariton amplitude, $|H_y|\sim 4\sqrt{-X/\pi}$ and $|\partial_X H_y|\sim 2/\sqrt{-\pi X}$ as $X\to 0^-$. Consequently, both H_y and the surface current J_x vanish continuously as $\sqrt{-x}$ at the edge, whereas their longitudinal derivative, which determines the normal electric field $E_z=i\partial_x H_y/(\omega\epsilon_b)$ and the surface charge density, diverges

as $(-x)^{-1/2}$. Meanwhile, the tangential electric field $E_x = J_x/\sigma$ vanishes as $\sqrt{-x}$ along with the current.

Figure 4 illustrates both the global standing-wave profile and the local near-edge scaling. In Fig. 4(a), we plot the normalized surface magnetic and electric fields, $|H_y|$ and $|\partial_X H_y| = (\omega\epsilon_b/\kappa)|E_z|$, respectively, against the normalized distance $-x/\lambda_{\mathrm{sp}}$. Here, $\lambda_{\mathrm{sp}} = 2\pi/\kappa$ is the polariton wavelength, so that $s = -X = 2\pi(-x/\lambda_{\mathrm{sp}})$. While the bound-wave component alone remains finite at $x = 0$, adding the sheet-side continuum brings the total magnetic trace sharply to zero at the termination. Farther from the edge ($s \gg 1$), the small-t behavior $\rho(t) \sim t/(\sqrt{2}\pi)$ governs the integral in Eq. (15), causing the continuum correction to decay rapidly as $\sin(s + \pi/8) - \psi(s) \sim (\sqrt{2}\pi s^2)^{-1}$, beyond which the bound polariton standing wave dominates. Figure 4(b) confirms that close to the termination ($-X \ll 1$), $|H_y|$ and $|\partial_X H_y|$ follow the analytical asymptotes $4\sqrt{-X/\pi}$ and $2/\sqrt{-\pi X}$. Taken together, Figs. 1-4 show how modal completeness, the reflection phase shift, and continuous current termination are unified within a single CMT solution.

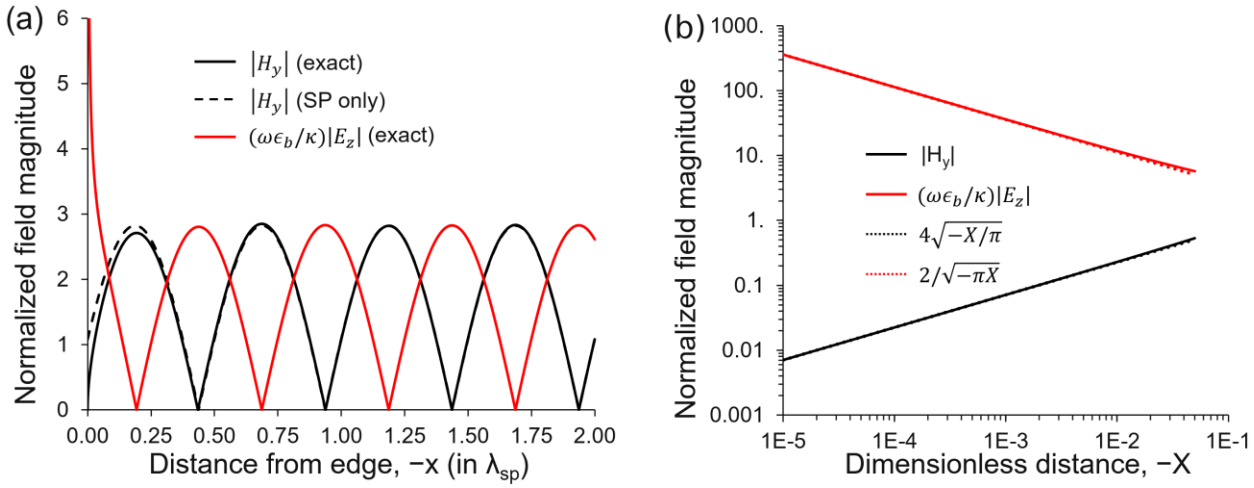


Figure 4: Surface electric and magnetic fields, and near-edge scaling for unit incident polariton amplitude. (a) Exact magnetic and normal electric fields (solid curves), together with the bound-polariton contribution to $|H_y|$ (dashed). (b) Near-edge behavior, $|H_y| \propto \sqrt{-X}$ and $|\partial_X H_y| \propto (-X)^{-1/2}$. The dotted lines are the analytical asymptotes.

Conclusion

In conclusion, we have presented a complete coupled-mode theory (CMT) analysis of surface-polariton (SP) reflection at the edge of a two-dimensional (2D) conducting sheet, connecting the far-field reflection phase shift directly to the excitation of near-edge evanescent continua. By expressing the boundary matching conditions in terms of orthonormal transverse eigenvectors, we showed that eliminating the continuum amplitudes yields a positive effective reactive response that separates the contributions of the empty-side and sheet-side continua and fixes the negative sign of the phase correction produced when the sheet-side modes are restored. By solving the coupled modal equations analytically in the quasistatic limit, we obtained the exact continuum spectra, and showed that the sheet-side continuum reduces the reactive boundary response from $2/\pi$ to $\sqrt{2}-1$ and shifts the reflection phase to $\pi/4$. Furthermore, we demonstrated that the complete sheet-side continuum cancels the bound-wave surface current at the edge, while its high-momentum tail determines the square-root current profile and the accompanying $(-x)^{-1/2}$ singularity in the normal electric field. These findings unite the analytical exactness of the Wiener-Hopf method with the physical transparency of the complete modal method, providing exact continuum spectra for assessing CMT calculations of 2DSP scattering and quantitative phase-convergence criteria for the one-sided cutoff scheme considered here.

Appendix A. Normalization and the retarded modal equations

The transverse eigenvectors defined in Eq. (3) form complete orthonormal bases on the half-line $Z>0$. Specifically, the sheet-side wavefunctions $\langle Z|p\rangle$ and $\langle Z|a_t\rangle$ obey the boundary condition $\partial_Z H=-H$ at $Z=0$, whereas the empty-side wavefunctions $\langle Z|f_q\rangle$ obey $H=0$ at $Z=0$. Their inner products satisfy the orthonormality and completeness relations,

$$\langle p|p\rangle=1,\quad \langle p|a_t\rangle=0,\quad \langle a_t|a_u\rangle=\delta(t-u),\quad \langle f_q|f_u\rangle=\delta(q-u),$$
$$|p\rangle\langle p|+\int_0^\infty |a_t\rangle\langle a_t|\,dt=\int_0^\infty |f_q\rangle\langle f_q|\,dq=\hat{I}. \tag{17}$$

The coupling overlap $W(q,t) = \langle f_q | a_t \rangle$ in Eq. (5) follows directly from sine–sine orthogonality and the standard principal-value integral $\int_0^\infty \sin(qZ)\cos(tZ)\, dZ = \mathrm{PV}[q/(q^2 - t^2)]$.

When retardation is retained ($\nu = k_b/\kappa > 0$) at normal incidence, the longitudinal propagation constants become $\gamma_0 = \sqrt{1+\nu^2}$ for the bound polariton and $\gamma(t) = \sqrt{\nu^2 - t^2}$ (with $\mathrm{Re}\,\gamma \geq 0$ and $\mathrm{Im}\,\gamma \geq 0$) for the continuum modes. The field states in Eq. (4) then generalize to

$$|H_L(X)\rangle = [e^{i\gamma_0 X} - Re^{-i\gamma_0 X}]|p\rangle - \int_0^\infty \alpha_t |a_t\rangle e^{-i\gamma(t)X}\, dt,$$
$$|H_R(X)\rangle = \int_0^\infty \phi_q |f_q\rangle e^{i\gamma(q)X}\, dq, \tag{18}$$

and projecting the continuity conditions at $X = 0$ yields the retarded integral equation for ϕ_q,

$$\gamma(q)\phi_q + \int_0^\infty [\gamma_0 P(q)P(u)^* + \int_0^\infty \gamma(t)W(q,t)W(u,t)^*\, dt]\phi_u\, du = 2\gamma_0 P(q). \tag{19}$$

Here, the range $0 < t < \nu$ corresponds to propagating radiation modes that carry power into free space, whereas $t > \nu$ corresponds to evanescent continuum modes. Taking $\nu \to 0$ ($\gamma_0 \to 1$, $\gamma(t) \to it$) reduces Eqs. (18) and (19) to the quasistatic equations in the main text.

Finally, for comparison with other reflection phase conventions in the literature under the $e^{-i\omega t}$ time dependence, the reflection coefficients of the individual electromagnetic field components and the quasistatic potential φ are related to R by

$$r_{H_y} = r_{J_x} = r_{E_x} = -R = e^{-3i\pi/4}, \quad r_{E_z} = r_\varphi = R = e^{i\pi/4}, \tag{20}$$

where the sign change between r_{E_z} and r_{H_y} arises from differentiating the oppositely propagating incident (e^{iX}) and reflected (e^{-iX}) waves with respect to x. Equation (20) specifies the component conventions when comparing phases with Refs. [6,8,9].

Appendix B. Construction of the exact continuum solution

In this appendix, we summarize the analytical derivation of the exact continuum spectra in Section 3. We note that the underlying quasistatic boundary problem is equivalent, after rescaling and reflecting the longitudinal coordinate, to the mixed boundary problem analyzed in Ref. [16]. In the real standing-wave representation corresponding to Eq. (13), the empty-side magnetic field for $X > 0$ is expanded as $h_R(X,Z) = \int_0^\infty B(q)e^{-qX}\sin(qZ)\,dq$, where $B(q)$ denotes the real empty-side spectral density. Projecting the continuity of $h_L(0,Z) = h_R(0,Z)$ and its longitudinal derivative $-\partial_s h_L(0,Z) = \partial_X h_R(0,Z)$ at $X = 0$ onto the sine basis $\sin(qZ)$ yields two coupled relations,

$$\begin{aligned} B(q) &= \frac{2q\sin\theta}{\pi(1+q^2)} - \frac{2q}{\pi}\,\mathrm{PV}\int_0^\infty \frac{\rho(t)}{q^2-t^2}\,dt + \frac{\rho(q)}{q}, \\ qB(q) &= \frac{2q\cos\theta}{\pi(1+q^2)} + \frac{2q}{\pi}\,\mathrm{PV}\int_0^\infty \frac{t\rho(t)}{q^2-t^2}\,dt - \rho(q). \end{aligned} \tag{21}$$

Eliminating the empty-side density $B(q)$ between the two lines of Eq. (21) produces a single Cauchy singular integral equation for the sheet-side density $\rho(t)$,

$$\mathrm{PV}\int_0^\infty \frac{\rho(t)}{t-q}\,dt + \frac{\pi}{q}\rho(q) = \frac{\cos\theta - q\sin\theta}{1+q^2}, \quad q > 0. \tag{22}$$

To solve Eq. (22), we introduce the Cauchy transform $C(\zeta) = \int_0^\infty \rho(t)/(t-\zeta)\,dt$ for complex ζ not on the nonnegative real axis. By the Plemelj formula [17], its boundary values $C_\pm(q) = \mathrm{PV}\int_0^\infty \rho(t)/(t-q)\,dt \pm i\pi\rho(q)$ convert Eq. (22) into the boundary condition $(q-i)C_+(q) + (q+i)C_-(q) = 2q(\cos\theta - q\sin\theta)/(1+q^2)$ on the positive real axis. Physical regularity at the edge requires $C(\zeta)$ to decay as $O(\zeta^{-1})$ at infinity away from the branch cut. Specifically, an additional homogeneous solution term would introduce a $t^{-1/2}$ continuum tail, leading to $H_y \sim r^{-1/2}$ and $|\mathbf{E}| \sim r^{-3/2}$ at a distance r from the edge. Because such a branch violates both the boundedness of the magnetic trace and the finiteness of the local electric-field energy per unit edge length, excluding it leaves an integrable spectral density and ensures the $O(\zeta^{-1})$ decay. Introducing the canonical logarithmic integral $F(w) = \frac{1}{\pi}\int_0^\infty \log(w+t)/(1+t^2)\,dt$, which

coincides with $\eta(q)$ in Eq. (14) for $w = q > 0$ and satisfies $(q - i)e^{F(-q-i0)} + (q + i)e^{F(-q+i0)} = 0$ across the cut, we obtain the solution satisfying this regularity condition,

$$C(\zeta) = \frac{\cos\theta - \zeta\sin\theta - Ae^{F(-\zeta)}}{1 + \zeta^2}, \quad F(w) = \frac{1}{\pi}\int_0^\infty \frac{\log(w + t)}{1 + t^2}\, dt, \tag{23}$$

where A is a constant. Because $C(\zeta)$ must remain analytic away from the nonnegative real axis, the numerator of Eq. (23) must vanish at the apparent poles $\zeta = \pm i$ of the denominator. Since $F(\pm i) = \frac{1}{2}\log 2 \pm i\pi/8$ (obtained by setting $t = \tan u$), pole cancellation at $\zeta = \pm i$ requires $e^{-i\theta} = A\sqrt{2}\, e^{-i\pi/8}$, which uniquely fixes the standing-wave phase and amplitude constant to $\theta = \pi/8$ and $A = 1/\sqrt{2}$.

Taking the Plemelj jump $\rho(t) = [C_+(t) - C_-(t)]/(2\pi i)$ across the positive real axis and substituting the result back into Eq. (21) yields the exact spectral densities on both sides of the edge,

$$\rho(t) = \frac{t\, e^{-\eta(t)}}{\sqrt{2}\,\pi(1 + t^2)}, \quad B(q) = \frac{e^{\eta(q)}}{\sqrt{2}\,\pi(1 + q^2)}. \tag{24}$$

Multiplying the standing-wave fields by $-2i\sqrt{2}\, e^{i\pi/8}$ sets the incident polariton coefficient to unity and gives the complex modal amplitudes in Eq. (14). Physically, this solution selects the unique regular branch where $\rho(t) \sim t/(\sqrt{2}\pi)$ at small t and $\rho(t) \sim t^{-3/2}/(\sqrt{2}\pi)$ at large t, ensuring a vanishing surface current and integrable local electric-field energy at the termination. Here, the local electric-field energy refers to the two-dimensional cross-sectional integral per unit length along y, where $|\mathbf{E}| \sim r^{-1/2}$ for the regular branch so that $\int |\mathbf{E}|^2 r\, dr\, d\vartheta$ remains finite near the edge (whereas the one-dimensional surface line integral $\int |E_z(x, 0^+)|^2\, dx$ diverges logarithmically and does not represent the physical energy condition).

For rapid and accurate numerical evaluation across all momenta, integration by parts and variable inversion provide two convenient identities for $\eta(t)$,

$$\eta(t) = \frac{1}{4}\log(1 + t^2) - \frac{1}{\pi}\int_0^t \frac{\log(u)}{1 + u^2}\, du, \quad \eta(t) = \frac{1}{2}\log(t) + \eta(1/t), \tag{25}$$

where the first form is used for $0 < t \leq 1$ and the reciprocal identity on the right stabilizes the evaluation for $t > 1$. Finally, expanding $C(\zeta)$ in Eq. (23) at large $|\zeta|$, where $C(\zeta) \sim -\zeta^{-1} \int_0^\infty \rho(t)\, dt$, directly yields the surface current sum rule $\int_0^\infty \rho(t)\, dt = \sin(\pi/8)$ in Eq. (15).

Acknowledgements

This work was supported by the National Research Foundation of Korea (NRF) grant funded by the Korean government (MSIT) (NRF-RS-2024-00454528).

References

[1] D. N. Basov, M. M. Fogler, and F. J. García de Abajo, Polaritons in van der Waals materials, Science **354**, aag1992 (2016).

[2] T. Low, A. Chaves, J. D. Caldwell, A. Kumar, N. X. Fang, P. Avouris, T. F. Heinz, F. Guinea, L. Martin-Moreno, and F. Koppens, Polaritons in layered two-dimensional materials, Nature Materials **16**, 182 (2017).

[3] Z. Fei et al., Gate-tuning of graphene plasmons revealed by infrared nano-imaging, Nature **487**, 82 (2012).

[4] J. Chen et al., Optical nano-imaging of gate-tunable graphene plasmons, Nature **487**, 77 (2012).

[5] J. Chen et al., Strong Plasmon Reflection at Nanometer-Size Gaps in Monolayer Graphene on SiC, Nano Lett. **13**, 6210 (2013).

[6] A. Y. Nikitin, T. Low, and L. Martin-Moreno, Anomalous reflection phase of graphene plasmons and its influence on resonators, Phys. Rev. B **90**, 041407 (2014).

[7] B. Rejaei and A. Khavasi, Scattering of surface plasmons on graphene by a discontinuity in surface conductivity, Journal of Optics **17**, 075002 (2015).

[8] B. Jiang et al., Theory of plasmon reflection by a 1D junction, Opt. Express **26**, 17209 (2018).

[9] J. H. Kang, S. Wang, Z. Shi, W. Zhao, E. Yablonovitch, and F. Wang, Goos-Hänchen Shift and Even–Odd Peak Oscillations in Edge-Reflections of Surface Polaritons in Atomically Thin Crystals, Nano Lett. **17**, 1768 (2017).

[10] A. J. Chaves, B. Amorim, Y. V. Bludov, P. A. D. Gonçalves, and N. M. R. Peres, Scattering of graphene plasmons at abrupt interfaces: An analytic and numeric study, Phys. Rev. B **97**, 035434 (2018).

[11] J. H. Kang, S. Wang, and F. Wang, Tunneling of two-dimensional surface polaritons through nanogaps in atomically thin crystals, Phys. Rev. B **99**, 165408 (2019).

[12] S. Lee and J. H. Kang, Theory of two-dimensional surface polaritons and their propagation, J. Korean Phys. Soc. **86**, 827 (2025).

[13] M. B. Lundeberg et al., Tuning quantum nonlocal effects in graphene plasmonics, Science **357**, 187 (2017).

[14] Rajendra Bhatia, *Positive Definite Matrices* (Princeton University Press, Princeton, NJ, 2007), Chap. 1.

[15] J. Meixner, The behavior of electromagnetic fields at edges, IEEE Trans. Antennas Propag. **20**, 442 (1972).

[16] T. Kulczycki, M. Kwaśnicki, J. Małecki, and A. Stos, Spectral properties of the Cauchy process on half-line and interval, Proceedings of the London Mathematical Society **101**, 589 (2010).

[17] H. W. Wyld, *Mathematical Methods for Physics: 45th Anniversary Edition*, (CRC Press, Boca Raton, FL, 2021), Secs. 13.2–13.3.